Ickrath, M., Bohnhoff, M., Bulut, F., Dresen, G. (2014): Stress rotation and recovery in conjunction with the 1999 Izmit Mw 7.4 earthquake. - Geophysical Journal International, 196, 2, pp. 951—956.

DOI: http://doi.org/10.1093/gji/ggt409

Geophysical Journal International

Geophys. J. Int. (2014) **196,** 951–956
Advance Access publication 2013 November 2

doi: 10.1093/gji/ggt409

Stress rotation and recovery in conjunction with the 1999 Izmit M_w 7.4 earthquake

M. Ickrath,[1] M. Bohnhoff,[1,2] F. Bulut[1] and G. Dresen[1]

[1] *Helmholtz Centre Potsdam,GFZ German Research Centre for Geosciences Section* 3.2, *Geomechanics and Rheology, Telegrafenberg,* D-14473 *Potsdam, Germany. E-mail: ickrath@gfz-potsdam.de*
[2] *Free University Berlin, Department of Earth Sciences, Malteser Strasse* 74-100, 12249 *Berlin, Germany*

Accepted 2013 October 2. Received 2013 September 30; in original form 2013 July 12

SUMMARY

Local rotations of the stress field might serve as an indicator to characterize the physical status of individual fault segments during the seismic cycle. In this study we focus on the pre-, 2-month aftershock- and post-seismic phase of the 1999 M_w7.4 Izmit earthquake in north-western Turkey. Using a compilation of focal mechanism data we investigate spatiotemporal changes of the stress field orientations and find distinct variations along individual fault segments. Whereas the regional stress field prior to the Izmit earthquake and following the 2-month aftershock sequence reflects a stable strike-slip regime, the early aftershock period is dominated by EW-extension below the Akyazi Basin. During the 2-month aftershock period we find significant changes from strike-slip to normal-faulting during the main shock following by a systematic backrotation to the pre-main shock stress regime. This backrotation commences first in the Akyazi Plain hosting a co-seismic slip deficit of $\leq$3 m and propagates then further to the east towards the Karadere and Düzce faults where the Düzce M_w 7.1 main shock nucleated 87 d later. Our results confirm that spatiotemporal stress field rotations are a useful indicator for variations of the seismotectonic setting during the seismic cycle.

Key words: Spatial analysis; Seismic cycle; Earthquake dynamics; Seismicity and tectonics; Transform faults.

GJI Seismology

1 INTRODUCTION

Spatial and temporal variations of the crustal stress field orientation related to fault activation may serve as an indicator to characterize the physical status of individual fault segments within the seismic cycle. However, stress field variations are extremely difficult to detect since the accuracy of stress inversion results is usually limited. Often, the error bounds in stress field orientation are of the same order of, or only slightly less than the amplitude of, the expected rotations. Studies along major fault ruptures ($M \sim 7$) indicate variations in stress orientation in the order of 10°–20° (e.g. Michael 1987a; Hauksson 1994; Zhao *et al.* 1997) but it was shown that such rotations should be interpreted with care (Townend & Zoback 2001). Recently, Hasegawa *et al.* (2011) and Hardebeck (2012) have observed significant rotations of the crustal stress field orientation exceeding up to 20° in conjunction with $M > 8.7$ earthquakes (Sumatra-Andaman/Indonesia 2004, Maule/Chile 2010, Tohoku-Oki/Japan 2011). These rotations imply a near-complete stress drop during the main shock and were followed by a rapid backrotation of the stress axes within months after the main shock. These studies confirmed the existence of stress rotations indicating that the amplitude of rotation is clearly observable for extremely large earthquakes. The Hasegawa *et al.* (2011) and Hardebeck (2012) case studies would support the recovery stress model first proposed by Michael (1987a), who suggested that the state of stress after the main shock returns rapidly back to the pre-main shock stress state. Another approach, the stress decay model by Hauksson & Jones (1988), comprises the suggestion that the average post-main shock stress change is of the same magnitude as the co-seismic stress drop and that there is a general decrease of the average stress recovering on the long-term similar to the tectonic reloading. In this study, we investigate potential spatiotemporal variations of the crustal stress field orientation along the 1999 Izmit M_w 7.4 earthquake in NW Turkey and relate our findings to distinct seismotectonic features and variations of co-seismic slip along the rupture. The Izmit event ruptured a ~140-km-long segment of the North Anatolian Fault Zone (NAFZ) in NW Turkey reflecting a right-lateral strike-slip mechanism consistent with the long-term regional stress field and a clear segmentation along its rupture (e.g. Tibi *et al.* 2001; Barka *et al.* 2002; Fig. 1A). Örgülü (2011) studied the stress field of the Marmara Sea region, which is mainly governed by a strike-slip regime. Here, we study the spatiotemporal evolution of the stress field orientations along the Izmit rupture by using a significantly enlarged aftershock focal mechanism (FM) data

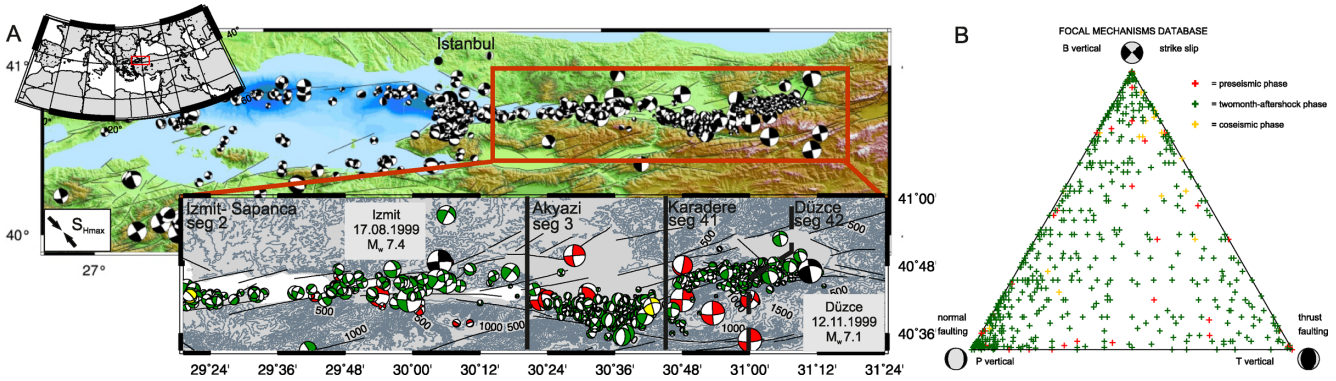

Figure 1. (A) Overview map of the focal mechanism (FM) database for the area of investigation at the North Anatolian Fault Zone in NW Turkey (please find the FM database in Table S1). The size of the beachballs scales with magnitude. Fault lines are taken from Turkey General Directorate of Mineral Research and Exploration, and Armijo *et al.* (2002). [Topography: SRTM30 grid, Bathymetry: Armijo *et al.* (2002), S_{Hmax}: Kiratzi (2002)]. Subplot: 656 FM along the Izmit rupture. Beachballs are colour-coded with time: prior to 1999 August, 1999 August–November and post 1999 November in red, green and yellow, respectively. Black beachballs represent the Izmit and Düzce main shocks. Black vertical lines indicate the segmentation along the Izmit rupture following Bohnhoff *et al.* (2006). Grey contour lines are isolines of topography. (B) Dipping angle of the *P*, *T* and *B* axes of all 939 FM visualized in a ternary scheme after Frohlich (2001) showing individual faulting mechanisms colour-coded with time.

base and additionally post-Izmit events allowing studying detailed temporal stress field variations along distinct rupture segments before, during and following the 2-month Izmit aftershock period.

2 METHOD AND DATA

There are several stress inversion algorithms, which estimate the orientation of the principal stress axes from FM data. Only four independent components can be obtained from stress tensor inversion, the orientation of the three principal stresses (σ_{1-3}) and the stress ratio $R = (\sigma_1 - \sigma_2)/(\sigma_1 - \sigma_3)$ ($0 \leq R \geq 1$ with $R < 0.5$ and $R > 0.5$ indicating a transtensional and transpressional regime, respectively). The different stress inversion methods were extensively discussed in the literature (e.g. Michael 1984; Gephart 1990; Hardebeck & Hauksson 2001; Abers & Gephart 2001). The standard methods generally provide similar results for the best-fitting stress tensor while error estimations vary between them (Hardebeck & Hauksson 2001; Bohnhoff *et al.* 2004). Here we use the technique proposed by Michael (1984, 1987b) designed based on a least-square inversion algorithm, which uses the orientation of a set of fault planes (strike and dip) and the direction of slip (rake) that occurs on these fault planes. Given this, the inversion method determines the best-fitting stress tensor by using a least-squares method minimizing the angle between the predicted tangential traction on the fault plane and the observed slip direction. Additionally, we also use the new developed software package MSATSI based on the Stress Inversion algorithm SATSI (Hardebeck & Michael 2006), which is a damped inversion method that simultaneously invert for the stress field orientations in subareas while minimizing the difference in stress between adjacent subareas. MSATSI has a user-friendly interface using MATLAB environment with a significant overall performance, stability improvement and comprehensive error handling (Martínez-Garzón *et al.*, in review). Compared to the Michael code, the damped inversion removes possible stress rotation artefacts exhibited by an undamped inversion and better resolves true stress rotations than a moving-window inversion. We use FM of local seismicity from pre-, 2-month aftershock- and post-seismic times framing the Izmit event, which are observed by various available local and regional seismic networks. We compiled a set of 939 FM of earthquakes along the broader Izmit rupture spanning the time interval 1943–2007 with earthquake magnitudes ranging between 0.8 and 7.4 (Figs 1 and 2). Individual data sets are compiled from Bohnhoff *et al.* (2006), Örgülü (2011), Görgün *et al.* (2010) and references therein (please find the FM database in Table S1). While the majority of events are aftershocks from the first 2 months following the Izmit main shock (Fig. 2b) we also include major regional events since 1943 (56 events) as well as seismicity following the 2-month aftershock activity between 2000 and 2007 (19 events). *P* and *T* axes of the entire FM data set show predominantly vertical but also subhorizontal compressional axes while extensional axes are mostly subhorizontal (Fig. 2a). This would reflect a combined strike-slip and normal faulting stress regime. In order to determine potential temporal variations in the stress field we divided the entire data set into a pre-, 2-month aftershock- and post-seismic period and then further subdivided the aftershock period into finer temporal subsets forming moving windows of 70 events with an overlap of 65 events. These subsets were separately inverted for the stress tensor using Michael and as comparison under same condition as one inversion with 108 grids consisting each of 70 FM with the MSATSI Software. Furthermore, within the Izmit aftershock period we also individually analysed the major rupture segments 2–4 defined by Bohnhoff *et al.* (2006; indicated in Fig. 1A subplot) . Segment 2 (29.3°E–30.4°E) includes the Izmit hypocentre and covers the Izmit–Sapanca area containing 122 FM dominated by a right-lateral strike-slip and minor normal faulting regime. Segment 3 (30.4°E–30.85°E) is located at a triple junction of the EW-striking Izmit–Sapanca Fault, the N65°E striking Karadere Fault and the ESE-striking Mudurnu Fault. It contains 170 FM, which mostly indicate an EW-extensional normal faulting regime. Segment 4 (30.85°E–31.3°E) extends along the Karadere Fault and the Düzce Basin containing 318 FM, which show a high variety in mechanism from strike-slip to normal faulting. For further analysis we separated this area into segments 41 (Karadere Fault, 115 FM) and 42 (Düzce Basin, 224 FM). To quantify the robustness of each derived stress tensor we also applied a bootstrap technique resampling 2000 times thereby determining the 68 per cent (1σ) and 95 per cent (2σ) confidence intervals.

3 RESULTS AND DISCUSSION

Results from both inversion algorithms are in good agreement reflecting for the broader Izmit/Düzce regions a strike-slip regime that

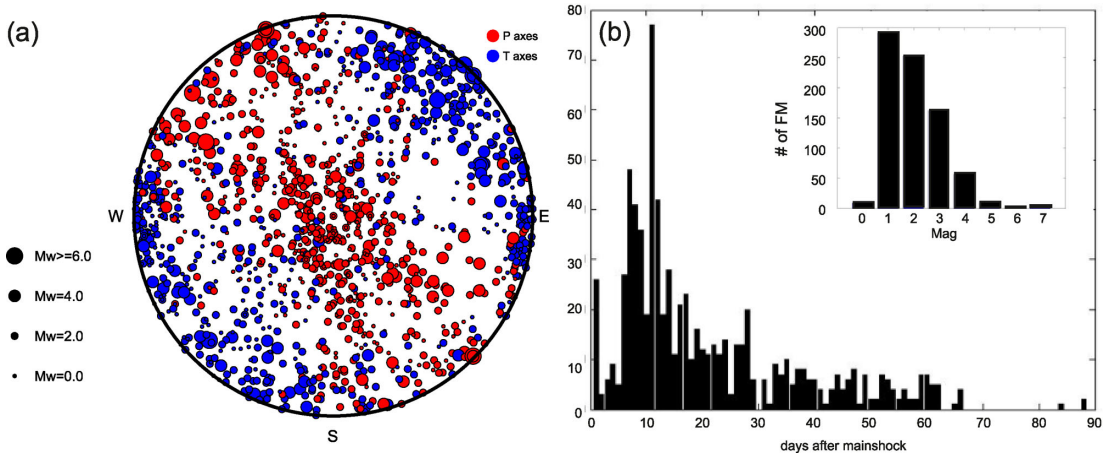

Figure 2. (a) Distribution of *P* (red) and *T* (blue) axes for the entire set of 939 FM in polar projection of the lower hemisphere. The size of circles scales with magnitude. (b) Event–time plot for the FM database for the 2-month Izmit aftershock period and its magnitude distribution (upper right-hand side).

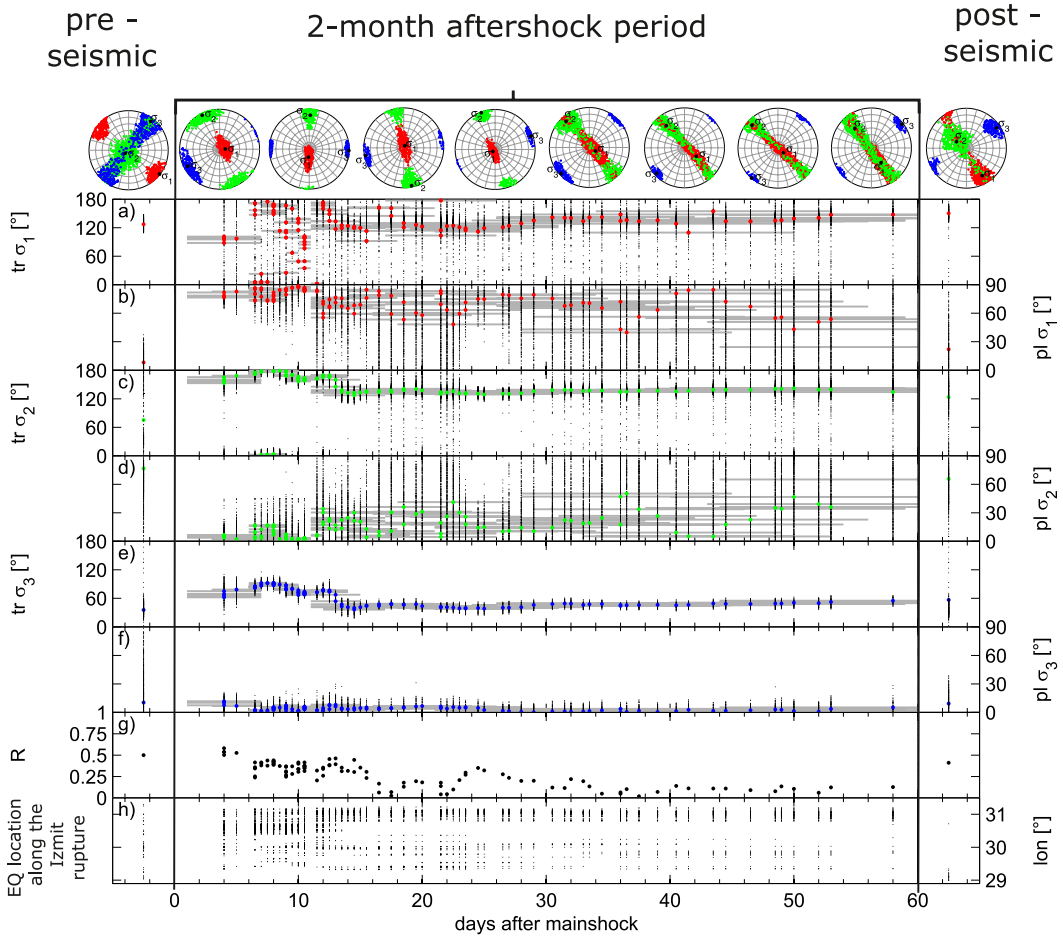

Figure 3. Temporal evolution of the stress field for the pre-, 2-month aftershock- and post-seismic phase of the Izmit earthquake. Significant stress tensor results from inversion for specific time periods are shown in lower hemisphere projection. Red: maximum compressive stress, σ_1. Green: intermediate principal stress, σ_2. Blue: minimum compressive stress, σ_3. Best solution is indicated by a black dot with 95 per cent uncertainty distribution from bootstrap resampling. (a–f) Best solutions for the stress tensor from each subset are plotted for the trend and plunge for σ_1 (red), σ_2 (green) and σ_3 (blue) with time. The horizontal grey bars are representing the temporal extent of each particular subset. For each result the 95 per cent confidence limit is plotted vertically. (g) Relative stress magnitude for the best solutions of each subset. (h) Spatial distribution of Izmit aftershocks along the rupture for each stress inversion subset.

remains almost identical during the pre- and post-seismic phases of the Izmit and Düzce 1999 events with a well-resolved N130°E trending subhorizontal maximum principal stress and a relative stress magnitude of ∼0.5 (Fig. 3). In contrast, during the 2-month aftershock sequence we observe significant lateral rotations of the trend of σ_{1-3} as well as significant changes for the plunge angle of σ_1 and σ_2 (but not σ_3) indicating temporal changes during the aftershock period. This observation confirms the stress field rotations

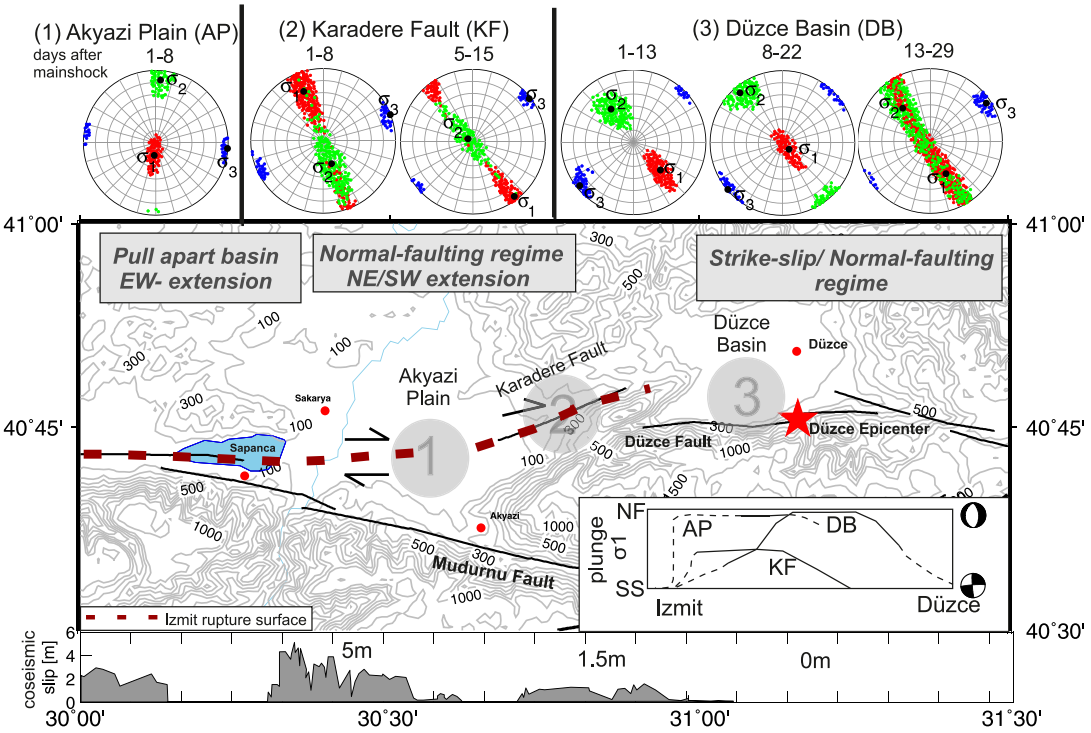

Figure 4. Upper part: Stress field orientations for segments 3 (Akyazi Plain, AP), segment 41 (Karadere Fault, KF) and 42 (Düzce Basin, DB) during the 2-month aftershock period (days with respect to the Izmit main shock). Labelling as in Fig. 3. Middle part: Summary of observations along the Akyazi and Düzce area. Faults are after Turkey General Directorate of Mineral Research and Exploration. Red dotted lines indicate the simplified surface rupture of the Izmit event (after Barka *et al.* 2002). The red star indicates the epicentre of the 1999 November 11 Düzce main shock. Grey: Contour lines for topography. Subplot: Sketch of principal results for the stress regime at the individual segments (AP, KF and DB, respectively), showing the temporal change of the plunge of the maximum compressive stress, σ_1 for the pre-, aftershock- and post-seismic phase of the Izmit earthquake and the significant change from SS (strike-slip) to NF (normal-faulting) and backwards in each segment with varying time delays. Lower part: Lateral distribution of co-seismic surface slip along the Izmit rupture after Barka *et al.* (2002).

introduced by the Izmit main shock that was first observed by Bohnhoff *et al.* (2006) along the Izmit-Sapanca and Karadere segments but with no temporal resolution. To further investigate the temporal evolution of the stress field orientation, and in particular taking into account the resolution capability, we plot the plunge and trend for σ_{1-3} as well as their 95 per cent confidence intervals individually with time (Figs 3a–f). Time extend of individual temporal subsets are indicated by horizontal grey lines in Fig. 3. For the aftershock data set as a whole, we identify an abrupt change in predominant faulting regime from the pre-seismic strike-slip to a normal faulting regime right after the main shock. During the 2-month aftershock period, we then observe a gradual but systematic backrotation with an intermitted transtensional stress field with overlapping confidence intervals of σ_1 and σ_2 and a relative stress magnitude <0.25. The compiled FM catalogue represents the entire rupture zone and all segments besides the Akyazi Plain are homogeneously sampled by FM for the entire time period (Fig. 3h). Towards the end of the 2-month aftershock period the stress field seems to return to the pre-seismic state (strike-slip) in agreement with the Michael (1987a) stress recovery model. However the reduced number of FM and their spatial distribution do not allow to draw concise conclusions in this aspect. During the 2-month aftershock period the relative stress magnitude changes from 0.5 to nearly 0, indicating a transtensional stress regime while it returns back to $\sim$0.4 in accordance with the backrotation of the stress field towards strike-slip with well-separated confidence regions of the principal stress axes (Fig. 3g). To further investigate the nature of the stress perturbation during the aftershock period we also investigated the temporal evolution of the stress field orientation focusing on the Akyazi Plain and the Karadere-Düzce area at the eastern part of the Izmit rupture (segments 3, 41 and 42; Fig. 1A subplot). Below the Akyazi Plain we identify a clear east–west extensional stress field with a vertical maximum principal stress orientation while the Karadere-Düzce area shows a distinctly varying stress field along the N65°E trending Karadere Fault and below the Düzce Basin (Fig. 4). The normal faulting regime below the Akyazi Plain is well explained by the co-seismic slip deficit of $\sim$3.5 m (Tibi *et al.* 2001; Barka *et al.* 2002) introducing a strong EW-trending tensional component in this area. This is also in accordance with the local tectonic setting reflecting an extensional basin structure with reduced topography by $\sim$500 m compared to the surrounding and thus may be seen as a structure similar to the somewhat larger Sea of Marmara pull-apart basin (Armijo *et al.* 2002) but in a more juvenile state. East of the Akyazi Plain, along the Karadere Fault we find a remarkable backrotation from oblique normal faulting towards strike-slip approximately 2 weeks after the Izmit main shock (Fig. 4 subplot). In contrast, below the Düzce Basin the regime changes from transtension/strike-slip towards NE-/SW-extensional normal faulting approx. 11 d after the main shock remaining constant for at least two week days and only then starting to rotate back to transtension/strike-slip (Fig. 4 subplot). Interestingly the significant changes in stress field orientation at Karadere and Dücze correlate with an unusual re-rise in seismicity rate $\sim$18 d after the main shock. Such a re-rise is not observed at the Akyazi Plain where the decay in aftershock activity entirely follows an Omori-decay Utsu (1961) in a stationary normal faulting stress regime (Fig. 4). We

explain these differences in temporal changes along the individual fault segments by the large variation of right-lateral co-seismic slip along the Izmit rupture. The slip deficit of ∼3.5 m with the highest gradient at the Akyazi Plain results in an immediate normal faulting activity reflected also by an $M > 5$ normal faulting aftershock a few hours following the main shock (Örgülü & Aktar 2001; Bulut *et al.* 2007). Once the slip deficit has been locally adjusted to a certain extent, the normal faulting activity vanishes and the tensional regime migrates further to the east where it continues to operate below the Düzce Basin but with a delay of several days (sketch in Fig. 4). The Karadere Fault in between does not switch to normal faulting since it represents a well-developed steeply NW-dipping strike-slip fault patch confirmed by the observed stress field orientation. The observed local temporal variations of the stress field orientations are significant at the 95 per cent level and in good accordance with the local tectonics along the particular segments of the Izmit rupture. In contrast, GPS-derived surface deformations do not show any significant temporal changes within the time considered here (Bürgmann *et al.* 2002; Ergintav *et al.* 2002). This might indicate that the adjustment of the slip deficit mainly occurs at seismogenic depth (8–18 km), but not up to the surface. Our results indicate a migration of the extensional stress regime from the Akyazi Plain that hosted the largest co-seismic slip deficit towards the Düzce Basin at the easternmost tip of the Izmit rupture. Interestingly this was the exact location where the M 7.1 Düzce rupture nucleated 87 d after Izmit extending the rupture by another 40 km to the east (Umutlu *et al.* 2004). Distinct local variations in the crustal stress field potentially reflect activity of a complex fault network varying in space and time. High-resolution stress inversion results allow unraveling fault processes at depth related to the temporal changes of geomechanical parameters.

4 CONCLUSIONS

We observe a systematic temporal variation of the crustal stress field orientation along distinct segments of the Izmit 1999 rupture during the 2-month aftershock period. We recognize a short-term change in the regional strike-slip stress field towards EW-extensional normal faulting along local pull-apart structures (Akyazi Plain, Dücze Basin). This would confirm the suggestion that shear failure and the associated drop in shear stress during large earthquakes may result in a rotation of the principal stresses acting on the fault along distinct patches and in accordance with lateral variations of co-seismic slip. No variation between the background stress field prior to the 1999 Izmit event and the post-seismic setting following the 2-month aftershock period (2000–2007) is observed indicating that the stress field rapidly recovers from a large earthquake as the aftershock rate decreases.

ACKNOWLEDGEMENTS

The study was funded by the Helmholtz Association in the frame of the Young Investigators Group 'From Microseismicity to Large Earthquakes'. We would like to thank Patricia Martínez-Garzón and Grzegorz Kwiatek for providing the MSATSI Software and for their support and helpful discussions. We thank the editor Jeannot Trampert and acknowledge comments by two anonymous reviewers. We thank John Townend for comments on an earlier version of the paper. We also like to thank the German Task Force for Earthquakes and especially J. Zschau and C. Milkereit for providing the Izmit aftershock waveform data.

REFERENCES

Abers, G.A. & Gephart, J.W., 2001. Direct inversion of earthquake first motions for both the stress tensor and focal mechanisms and application to southern California, *J. geophys. Res.,* **106**(B11), 26 523–26 540.

Armijo, R., Meyer, B., Navarro, S., King, G. & Barka, A., 2002. Asymmetric slip partitioning in the Sea of Marmara pull-apart: a clue to propagation processes of the North Anatolian Fault? *Terra Nova,* **14**(2), 80–86.

Barka, A. *et al.*, 2002. The surface rupture and slip distribution of the 17 august 1999 Izmit earthquake (M7.4), North Anatolian Fault, *Bull. seism. Soc. Am.,* **92**(1), 43–60.

Bohnhoff, M., Baisch, S. & Harjes, H.P., 2004. Fault mechanisms of induced seismicity at the Superdeep German Continental Deep Drilling Program (KTB) borehole and their relation to fault structure and stress field, *J. geophys. Res,* **109,** B02309, doi:10.1029/2003JB002528.

Bohnhoff, M., Grosser, H. & Dresen, G., 2006. Strain partitioning and stress rotation at the North Anatolian Fault zone from aftershock focal mechanisms of the 1999 Izmit Mw = 7.4 earthquake, *Geophys. J. Int.,* **166**(1), 373–385.

Bürgmann, R., Ergintav, S., Segall, P., Hearn, E., McClusky, S., Reilinger, R., Woith, H. & Zschau, J., 2002. Time-dependent distributed afterslip on and deep below the Izmit earthquake rupture, *Bull. seism. Soc. Am.,* **92**(1), 126–137.

Bulut, F., Bohnhoff, M., Aktar, M. & Dresen, G., 2007. Characterization of aftershock-fault plane orientations of the 1999 Izmit (Turkey) earthquake using high-resolution aftershock locations, *Geophys. Res. Lett.,* **34**, L20306, doi:10.1029/2007GL031154.

Ergintav, S., Bürgmann, R., McClusky, S., Çakmak, R., Reilinger, R.E., Lenk, O., Barka, A. & Özener, H., 2002. Postseismic deformation near the Izmit earthquake (17 August 1999, M 7.5) rupture zone, *Bull. seism. Soc. Am.,* **92,** 194–207.

Frohlich, C., 2001. Display and quantitative assessment of distributions of earthquake focal mechanisms, *Geophys. J. Int.,* **144,** 300–308.

Gephart, J.W., 1990. Stress and the direction of slip on fault planes, *Tectonics,* **9**(4), 845–858.

Görgün, E., Bohnhoff, M., Bulut, F. & Dresen, G., 2010. Seismotectonic setting of the Karadere-Düzce branch of the North Anatolian Fault zone between the 1999 Izmit and Düzce ruptures from analysis of Izmit aftershock focal mechanisms, *Tectonophysics,* **482,** 170–181.

Hardebeck, J., 2012. Coseismic and postseismic stress rotations due to great subduction zone earthquakes, *Geophys. Res. Lett.,* **39,** L21312, doi:10.1029/2012GL053438.

Hardebeck, J.L. & Hauksson, E., 2001. Stress orientations obtained from earthquake focal mechanisms: what are appropriate uncertainty estimates? *Bull. seism. Soc. Am.,* **91**(2), 250–262.

Hardebeck, J.L. & Michael, A.J., 2006. Damped regional-scale stress inversions: methodology and examples for southern California and the Coalinga aftershock sequence, *J. geophys. Res. Solid Earth,* **111,** B11310, doi:10.1029/2005JB004144.

Hasegawa, A., Yoshida, K. & Okada, T., 2011. Nearly complete stress drop in the 2011 Mw 9.0 off the pacific coast of Tohoku earthquake, *Earth Planets Space,* **6**(7), 703–707.

Hauksson, E., 1994. State of stress from focal mechanisms before and after the 1992 landers earthquake sequence, *Bull. seism. Soc. Am.,* **84**(3), 917–934.

Hauksson, E. & Jones, L., 1988. The July 1986 oceanside (Ml = 5.3) earthquake sequence in the continental borderland, southern California, *Bull. seism. Soc. Am.,* **78,** 1885–1906.

Kiratzi, A.A., 2002. Stress tensor inversions along the westernmost north anatolian fault zone and its continuation into the North Aegean Sea, *Geophys. J. Int.,* **151**(2), 360–376.

Michael, A.J., 1984. Determination of stress from slip data: faults and folds, *J. geophys. Res,* **89**(B13), 11 517–11 526.

Michael, A.J., 1987a. Stress rotation during the Coalinga aftershock sequence, *J. geophys. Res.,* **92,** 7963–7979.

Michael, A.J., 1987b. Use of focal mechanisms to determine stress: a control study, *J. geophys. Res.,* **92,** 357–369.

Örgülü, G., 2011. Seismicity and source parameters for small-scale earthquakes along the splays of the North Anatolian Fault (NAF) in the Marmara Sea, *Geophys. J. Int.*, **184**(1), 385–404.

Örgülü, G. & Aktar, M., 2001. Regional moment tensor inversion for strong aftershocks of the August 17, 1999 Izmit earthquake (Mw = 7.4), *Geophys. Res. Lett.,* **28**(2), 371–374.

Tibi, R. *et al.*, 2001. Rupture processes of the 1999 August 17 Izmit and November 12 Düzce (Turkey) Earthquakes, *Geophys. J. Int.,* **144**(2), F1–F7.

Townend, J. & Zoback, M.D., 2001. Implications of earthquake focal mechanisms for the frictional strength of the San Andreas fault system, in *The Nature and Significance of Fault Zone Weakening,* Vol. **186,** pp. 13–21, eds Holdsworth, R.E., Strachan, R.A., Macloughlin, J.F. & Knipe, R.J., Geol. Soc. London Spec. Publ.

Umutlu, N., Koketsu, K. & Milkereit, C., 2004. The rupture process during the 1999 Düzce, Turkey, Earthquake from joint inversion of teleseismic and strong-motion data, *Tectonophysics,* **391**(1–4), 315–324.

Utsu, T.A., 1961. A statistical study of the occurrence of aftershocks, *Geophys. Mag.,* **30,** 521–605.

Zhao, D., Kanamori, H. & Wiens, D., 1997. State of stress before and after the 1994 Northridge Earthquake, *Geophys. Res. Lett.,* **24**(5), 519–522.

SUPPORTING INFORMATION

Additional Supporting Information may be found in the online version of this paper:

Table S1
(http://gji.oxfordjournals.org/lookup/suppl/doi:10.1093/gji/ggt409/-/DC1)

Please note: Oxford University Press is not responsible for the content or functionality of any supporting materials supplied by the authors. Any queries (other than missing material) should be directed to the corresponding author for the article.